# Photoreduction of metal nanostructures on periodically proton exchanged MgO-doped lithium niobate crystals

Laila Balobaid,[1] N. Craig Carville,[1,2] Michele Manzo,[3] Liam Collins,[1,2] Katia Gallo,[3] and Brian J. Rodriguez[1,2,a)]

[1]*School of Physics, University College Dublin, Belfield, Dublin 4, Ireland*
[2]*Conway Institute of Biomolecular and Biomedical Research, University College Dublin, Belfield, Dublin 4, Ireland*
[3]*Department of Applied Physics, KTH-Royal Institute of Technology, Roslagstullbacken 21, 106 91 Stockholm, Sweden*

(Received 16 August 2013; accepted 15 October 2013; published online 30 October 2013)

Local reactivity on periodically proton exchanged lithium niobate (PPE:LN) surfaces is a promising route for the fabrication of regularly spaced nanostructures. Here, using MgO-doped PPE:LN templates, we investigate the influence of the doping on the nanostructure formation as a function of the proton exchange (PE) depth. The deposition is found to occur preferentially along the boundary between MgO-doped LN and the PE region when the PE depth is at least 1.73 $\mu$m, however, for shallower depths, deposition occurs across the entire PE region. The results are found to be consistent with an increased photoconductivity of the MgO-doped LN. © *2013 AIP Publishing LLC*. [http://dx.doi.org/10.1063/1.4827541]

Spatially defined metal nanowires and nanostructures with tunable properties are of interest for use in biological and chemical sensing and energy harvesting applications.[1–5] Ferroelectric substrates are promising templates for the fabrication of such nanostructures via ferroelectric lithography,[6,7] whereby the location of the nanostructures can be engineered by controlling the local polarization and deposition conditions. Such polarization-controlled metal nanostructure deposition has been demonstrated on domain-patterned $BaTiO_3$,[8,9] $PbZrTiO_3$,[10,11] and $LiNbO_3$ (LN)[12–18] surfaces.

For LN crystals, the bulk polarization can be reversed with an external field, or alternatively, the polarization in a shallow volume beneath the surface can be reduced via proton exchange (PE).[19,20] Exchanging regions of congruent LN with protons from a benzoic acid source yields $H_xLi_{1-x}NbO_3$ layers approaching the paraelectric $HNbO_3$ phase. Depending on the PE conditions, the $H_xLi_{1-x}NbO_3$ layers can exhibit various $Li^+-H^+$ exchange ratios ($x$), with different crystallographic phases.[21] Useful insights on the latter can be gained through optical characterizations (in particular by refractive index profiling and infrared absorption). During the PE process, lithium ions (and vacancies) are replaced by hydrogen ions, which penetrate into the crystal at the surfaces exposed to the acid, via a diffusion process yielding a PE depth well-described by the Arrhenius equation.[22]

Both aforementioned approaches (poling and PE) can be used to fabricate periodic arrays of either reversed ferroelectric domains or polarization-reduced regions across the crystal surface. Recently, we demonstrated that such periodic PE:LN templates[23,24] can be used to form arrays of Ag nanostructures[1,3] and that the width and height of the nanostructures can be controlled by the PE depth[25] and $AgNO_3$ concentration,[26] respectively.

A technique commonly employed to reduce the sensitivity of LN crystals to the photorefractive effect (i.e., optical damage) is MgO doping,[27] which also influences the PE process.[28,29] MgO doping of LN also leads to a shift of the UV absorption edge to higher energy[30,31] and increased photoconductivity,[32–35] factors which can influence the photodeposition process. Previously, Liu *et al.* determined that Mn doping extended the absorption into the visible spectrum, thus facilitating visible-light assisted Ag photodeposition;[36] however, there are no investigations of the role of MgO doping on the photochemical deposition of metallic nanostructures on LN. Therefore, in this study, we investigate the role of MgO doping of LN on the PE and photodeposition processes.

Periodically proton exchanged (PPE) templates were fabricated using 0.5 mm-thick $z$-cut 5 mol. % MgO-doped LN (MgO:LN) substrates (Roditi Ltd.). An acid-resistant 100 nm-thick Ti layer was first deposited on the $-z$ side of the crystals. Next, spin-coated photoresist was patterned (with a mask of 12.17 $\mu$m period and 50% duty cycle, similar to the procedure described in Ref. 24) so as to periodically expose the previously evaporated Ti layer. The samples were then dry etched with a mixture of $Cl_2$/Ar in a cryo-reactive ion etching (RIE) setup (Oxford Plasmalab 100), which removed Ti from the exposed areas, ultimately yielding the Ti mask to be used for the selective PE. An additional Ti layer was also deposited on the $+z$ face of the crystal to prevent PE on this surface. The crystals were then immersed in a melt of pure benzoic acid ($C_6H_5COOH$) at 200 °C for different exchange times ($t_{PE} = \{0.9, 3.5, 8.0, 14.2, 22.2, 32.0\}$ h) in order to obtain PPE templates with different PE depths ($d_{PE_z}$). The PE depth was determined optically by dark mode reflectivity measurements[37] using a prism coupler setup (Metricon 2010/M) on planar reference samples exchanged at the same time as the PPE samples. After the PE, the Ti mask layers were removed by wet etching for a few seconds in 48% dilute hydrofluoric acid ($HF:H_2O$).

The surface topography of the PPE templates was characterized using amplitude modulation atomic force

a)E-mail: brian.rodriguez@ucd.ie

 

microscopy (AFM) (Asylum Research, MFP-3D) with cantilevers having nominal resonant frequencies of 330 kHz and spring constants of 42 N/m (Nanosensors, PPP-NCH). Images were processed using 0th order flattening.

The UV absorption edge was measured in planar PE (with $t_{PE} = 32$ h) and virgin MgO:LN and LN crystals using a Cary500 spectrophotometer, in double-beam configuration with 0.2 nm resolution.

Prior to photodeposition, the samples were cleaned using ultra-sonication for 30 min divided equally in the following order: acetone, isopropanol, and milliQ water (18.2 MΩ/cm). The concentration of the $AgNO_3$ solution used (Sigma Aldrich) was adjusted to 0.01 M, from which 70 $\mu$l was pipetted onto the surface of each sample. To photoreduce the $Ag^+$ ions, a 254 nm-UV pen lamp (Spectroline) with 1400 $\mu W/cm^2$ nominal power output was placed at a fixed distance of 2 cm from the surface of the sample. Each sample was illuminated for 5 min.

The surface topography variations were characterized before and after photodeposition using AFM. The samples were cleaned (and reused) by gently rubbing the sample with lens paper and isopropanol prior to the sonication steps described above. AFM confirmed the removal of the nanostructures.

The PE depth increased from 0.46 to 2.47 $\mu$m with increasing exposure time to the benzoic acid, as shown in Table I.[38] Accordingly, the diffusion constant for PE in MgO:LN in the $z$-direction at 200 °C, $D_{PE_z}$, was determined to be $0.051 \pm 0.002$ $\mu m^2/h$ by fitting the data of Fig. 1(a).[22] We have previously reported $D_{PE_z} = 0.084 \pm 0.004$ $\mu m^2/h$ for congruent LN processed with the same PE conditions.[25] Thus, the MgO doping lowered the PE diffusion rate in the $z$-direction, consistent with the findings of Ref. 27. The PE process also proceeds laterally in the $x$-direction under the Ti mask (i.e., lateral diffusion (LD)), with a diffusivity, $D_{PE_x}$, to be evaluated for our configuration as well.

A schematic of the templates after PE with the Ti mask in place and a typical AFM topography image of a PPE MgO:LN surface ($d_{PE_z} = 2.47$ $\mu$m) following Ti mask removal are shown in Figs. 1(b) and 1(c), respectively. Three distinct regions are illustrated: (i) MgO:LN, which had been protected from direct PE by the Ti mask, (ii) RIE, which corresponds to the Ti mask openings, and (iii) LD, which corresponds to the PE proceeding laterally under the Ti mask and encroaching on the MgO:LN region. Thus, the final PE region comprises the RIE and LD regions, as labeled in Fig. 1(b). The RIE and LD regions are characterized by surface swelling, as shown previously.[2,25] The AFM topography images of three as-cleaned samples with different PE depths are shown in Figs. 2(a)–2(c). As a consequence of lateral diffusion under the Ti mask, the width of the LD regions increases ($0.17 \pm 0.02$, $0.36 \pm 0.04$, and $1.44 \pm 0.03$ $\mu$m) with increasing PE depth (0.46, 0.93, and 2.47 $\mu$m, respectively) at the expense of the MgO:LN region. A similar trend was already observed in undoped LN.[25] The widths of the LD regions ($d_{PE_x}$) were determined as the mean and standard deviation of measurements from 10 line profile cross-sections perpendicular to the periodic structure, and are shown in Table I. From these results, $D_{PE_x}$ for our configuration for MgO:LN was determined to be $0.016 \pm 0.001$ $\mu m^2/h$ as compared to $0.038 \pm 0.001$ $\mu m^2/h$ for undoped LN.[25] Also, for the $x$-direction, MgO:LN samples showed a lower diffusion constant, which is consistent with previous results of PE in $x$-cut substrates.[29]

After UV illumination, Ag nanostructures formed on the PPE MgO-doped templates. The AFM topography images of three post-photodeposition samples with different PE depths are shown in Figs. 2(d)–2(f). At first glance, the results appear comparable to those obtained on undoped LN,[25] as Ag nanostructures are deposited on LD regions (see, e.g., Fig. 2(d)). However, upon closer inspection, it was

TABLE I. The PE conditions of MgO:LN samples.

| Depth, $d_{PE_Z}$ ($\mu$m) | Time, $t_{PE_Z}$ (h) | Width, $d_{PE_x}$ ($\mu$m) |
|---|---|---|
| $0.46 \pm 0.01$ | 0.9 | $0.17 \pm 0.02$ |
| $0.93 \pm 0.01$ | 3.5 | $0.36 \pm 0.04$ |
| $1.41 \pm 0.12$ | 8.0 | $0.70 \pm 0.04$ |
| $1.73 \pm 0.03$ | 14.2 | $0.98 \pm 0.05$ |
| $2.06 \pm 0.04$ | 22.2 | $1.17 \pm 0.08$ |
| $2.47 \pm 0.20$ | 32.0 | $1.44 \pm 0.03$ |

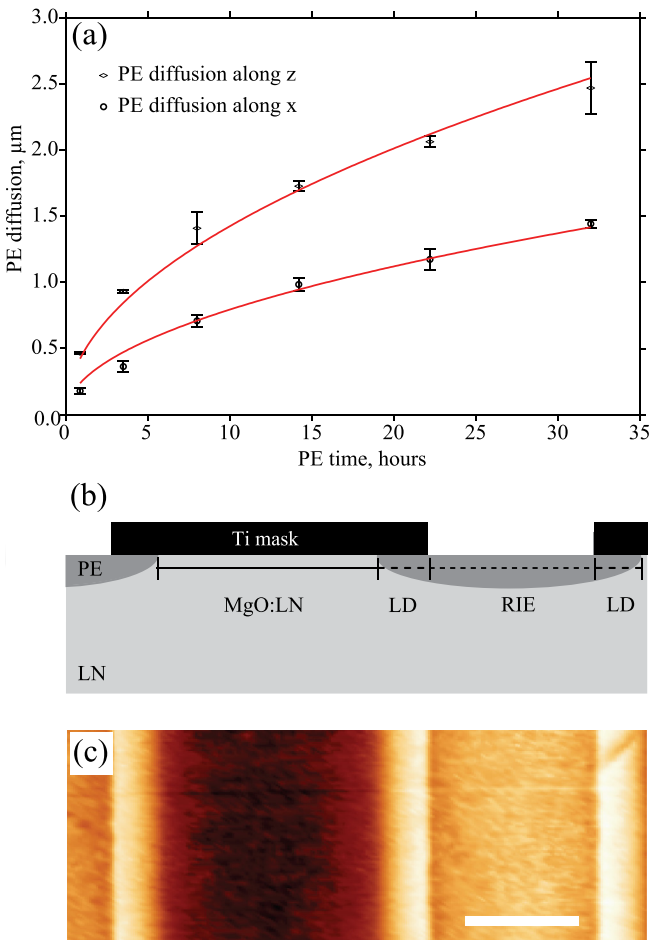


FIG. 1. (a) The measured thickness of the PE layers, $d_{PE_z}$, and $d_{PE_x}$, i.e., PE depth and LD width, respectively, plotted as a function of PE time, $t_{PE}$, for the PE temperature, $T_{PE} = 200$ °C. Solid lines represent curve fitting to $d_{PE} = \sqrt{4D_{PE}(T_{PE})t_{PE}}$ for z and x data. (b) A schematic of the PPE MgO:LN template prior to removal of the Ti mask. (c) AFM topography image of a PPE MgO:LN crystal surface with LN and PE regions defined ($d_{PE_z} = 2.47$ $\mu$m). The PE region comprises the RIE and LD regions. Scale bar in (c) indicates 3 $\mu$m. Vertical scale is 10 nm.

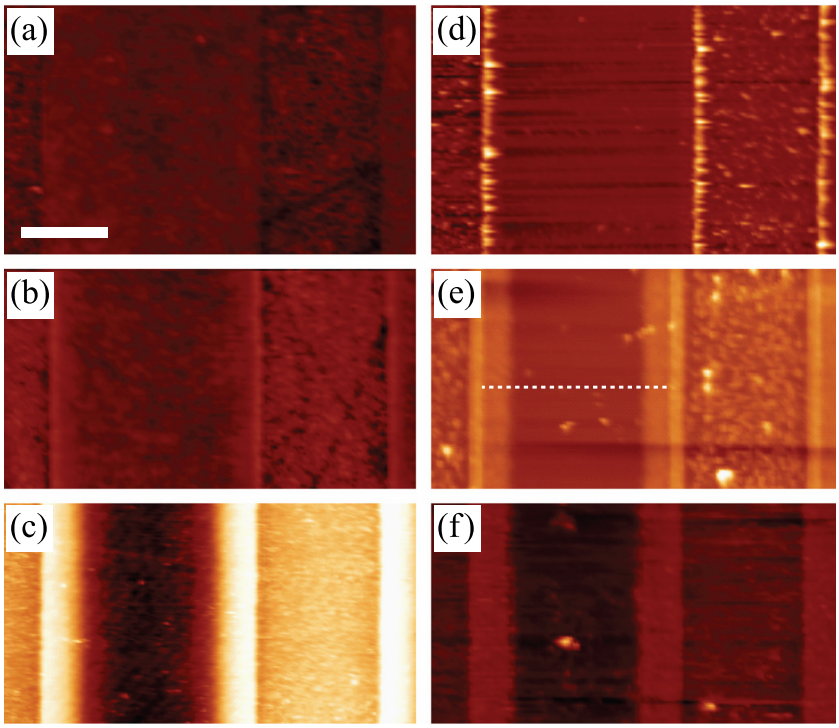


FIG. 2. AFM topography images of MgO-doped PPE:LN crystal surfaces for $d_{PE_z} = 0.46\,\mu$m, $0.93\,\mu$m, and $2.47\,\mu$m, (a)–(c) prior to photoreduction and (d)–(f) after photoreduction. Scale bar in (a) indicates $3\,\mu$m. Vertical scale is 10 nm for (a)–(c) and 100 nm for (d)–(f). The dashed white line in (e) indicates the width of the LN region for $d_{PE_z} = 0.93\,\mu$m.

determined that for some samples Ag nanostructures are also present in the RIE region. Fig. 3(a) shows the width of the deposited Ag nanostructures as a function of the PE depth. In the three shallowest PE depths ($d_{PE_z} < 1.73\,\mu$m), the width of deposited Ag nanostructures is at least as wide as the entire PE region, i.e., both the RIE and the LD regions. On the other hand, for the samples with the deepest PE depths, the deposition is confined to the LD regions only.

Interestingly, we have observed similar behavior in undoped PPE:LN samples, where the Ag nanostructures covered the entire PE region only for very shallow PE depths ($d_{PE_z} < 0.5\,\mu$m in undoped LN).[25] We attributed this feature to the interplay between the recombination of the photogenerated carriers and the location of the PE:LN interface along the $z$-direction, whereby for some critical depth, the photogenerated electrons would reach the surface under the influence of the electrostatic field arising from the bound-charge distribution at the buried PE:LN interface before recombining.[2,25] The results presented here on MgO-doped PPE:LN corroborate this hypothesis. Since the photoconductivity is larger (by several orders of magnitude) for MgO:LN vs. undoped LN,[32–35] the photogenerated electrons are also characterized by a longer recombination time as a result of the greatly reduced trapping cross section of $Fe^{3+}$ impurities for electrons.[32] In turn, this corresponds to pushing the critical PE:LN interface that can influence the photodeposition at the surface deeper into the crystal.

Another factor which may influence the photodeposition process is the UV absorption edge, which was measured to be ~326 and ~314 nm for LN and MgO:LN, respectively. The shift towards shorter wavelengths for MgO:LN is consistent with other studies.[30,31] Finally, the PE-induced UV absorption edge was measured to be roughly the same for both crystals (~346 and ~344 nm for LN and MgO:LN, respectively). Nevertheless, the shorter UV absorption edge implies the presence of fewer photogenerated charges in MgO:LN vs. LN templates and subsequently, should correspond to increased photodeposition on LN templates. This, however, is opposite to what is observed. Thus, the contribution of the increased photoconductivity of MgO:LN appears to be the mechanism that best supports the observed photodeposition behavior, as discussed before.

The average height of the deposited Ag nanostructures was determined with respect to the height difference between the swollen LD and the LN regions on the sample before deposition as the mean and standard deviation of measurements from 10 line profile cross-sections. As shown in Fig. 3(b), the average thickness of the Ag is $30.6 \pm 8.5$ nm for the LD region and $11.0 \pm 7.9$ nm for the RIE region for the sample with the shallowest PE depth (see inset (i) in Fig. 3(a)). These values decrease with increasing PE depth for the Ag thickness in the LD regions. For the RIE regions, the three deepest PE depths have negligible Ag deposition as shown schematically in inset (ii) of Fig. 3(a). In comparison, the average Ag height for the LD region of the undoped LN sample with the shallowest PE depth was $8.1 \pm 1.1$ nm. Thus, the MgO doping influences the final nanostructure thickness, a finding which is also supported by the increased photoconductivity of the MgO:LN.

Closer inspection of the after photodeposition images reveals that Ag deposits also in the LN region near the edge of the LD region for the sample having a PE depth of $0.93\,\mu$m (and $1.41\,\mu$m, data not shown). The dashed white line in Fig. 2(e) indicates the width of the LN region, thereby showing that the deposition occurs also in the LN region. Such behavior has not been observed on undoped samples. We also attribute this to the increased photoconductivity of the MgO:LN, which this time amplifies the action of the tangential component of the electrostatic fields stemming from the PE:LN boundary. Assuming in the first

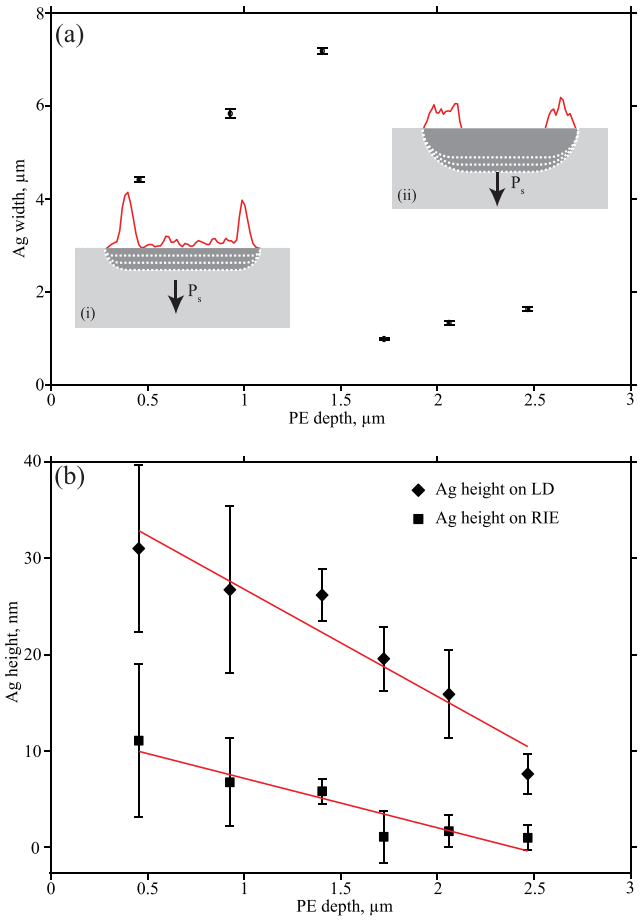


FIG. 3. (a) Width of Ag deposition plotted as a function of $d_{PE_z}$. Inset (i) is a schematic showing the three shallowest PE depths and a line profile of the Ag deposition for $d_{PE_z} = 0.46\,\mu$m, while inset (ii) is a schematic showing the three deepest PE depths and a line prolife of the Ag deposition for $d_{PE_z} = 2.47\,\mu$m (not to scale). The spontaneous polarization is labeled as $P_s$. (b) The mean ± standard deviation Ag deposition height within the LD and RIE regions and corresponding linear fits as a function of $d_{PE_z}$.

instance equivalent field distributions for undoped and MgO-doped substrates, the photoexcited electrons should be able to travel a longer distance away from the PE:LN edge before recombining, which in turn would result in a larger spatial extent of the Ag deposition reaching out further into the non-PE areas. The fact that this behavior is only observed for these particular depths is likely attributable to the interplay between the recombination of the photogenerated carriers and the location of the PE:LN interface along the *z*-direction, however, further work is needed to determine the underlying mechanism.

MgO doping was found to influence the photodeposition of Ag nanostructures onto chemically patterned LN crystal surfaces. Compared to the undoped case, the Ag nanostructures formed on the LD regions of PPE MgO:LN surfaces were thicker even for shorter UV illumination times. The increased thickness of the metal deposition may improve the sensitivity of applications based on arrays of nanowire sensors. Furthermore, Ag deposition occurred across the entire PE region for PE depths of less than 1.73 $\mu$m. For undoped LN, such behavior was observed only for the shallowest PE depth (0.59 $\mu$m). Finally, metal deposition was observed in the LN region at the PE:LN boundary, a behavior which was not observed for undoped LN. All of these observations are consistent with the increased photoconductivity of MgO:LN and the interplay between the recombination of the photogenerated carriers and the electric fields at the surface of the crystal. The increased photoconductivity of MgO:LN provides additional control over the shape and size of the resulting metallic nanostructures, and thus provides an additional route for tailoring the fabrication of complex metallic nanostructures on chemically patterned ferroelectric templates. Given the improved waveguide performance of MgO:LN compared to undoped LN, the demonstrated size-controlled fabrication of metallic nanostructures via photodeposition on MgO:LN provides a ferroelectric-metallic structure-based platform to exploit the plasmonic properties of the nanostructures simultaneously with the optical properties of the waveguides.

This publication has emanated from research conducted with the financial support of the DGPP and NANOREMEDIES, which are funded under the Programme for Research in Third Level Institutions (PRTLI) Cycle 5 and co-funded by the European Regional Development Fund. We also acknowledge support from the Swedish Research Council (VR 622-2010-526 and 621-2011-4040) and UCD Research. The AFM used for this work was funded by Science Foundation Ireland (No. SFI07/IN1/B931).

[1]Y. Cui, Q. Q. Wei, H. K. Park, and C. M. Lieber, Science **293**, 1289 (2001).
[2]N. C. Carville, M. Manzo, S. Damm, M. Castiella, L. Collins, D. Denning, S. A. L. Weber, K. Gallo, J. H. Rice, and B. J. Rodriguez, ACS Nano **6**, 7373 (2012).
[3]S. Damm, N. C. Carville, B. J. Rodriguez, M. Manzo, K. Gallo, and J. H. Rice, J. Phys. Chem. C **116**, 26543 (2012).
[4]S. Linic, P. Christopher, and D. B. Ingram, Nature Mater. **10**, 911 (2011).
[5]K. R. Catchpole and A. Polman, Opt. Express **16**, 21793 (2008).
[6]S. V. Kalinin, D. A. Bonnell, T. Alvarez, X. Lei, Z. Hu, J. H. Ferris, Q. Zhang, and S. Dunn, Nano Lett. **2**, 589 (2002).
[7]S. V. Kalinin, D. A. Bonnell, T. Alvarez, X. J. Lei, Z. Hu, R. Shao, and J. H. Ferris, Adv. Mater. **16**, 795 (2004).
[8]J. L. Giocondi and G. S. Rohrer, Chem. Mater. **13**, 241 (2001).
[9]J. L. Giocondi and G. S. Rohrer, J. Phys. Chem. B **105**, 8275 (2001).
[10]S. Dunn, P. M. Jones, and D. E. Gallardo, J. Am. Chem. Soc. **129**, 8724 (2007).
[11]D. Tiwari and S. Dunn, J. Mater. Sci. **44**, 5063 (2009).
[12]J. N. Hanson, B. J. Rodriguez, R. J. Nemanich, and A. Gruverman, Nanotechnology **17**, 4946 (2006).
[13]X. Liu, K. Kitamura, K. Terabe, H. Hatano, and N. Ohashi, Appl. Phys. Lett. **91**, 044101 (2007).
[14]S. Dunn and D. Tiwari, Appl. Phys. Lett. **93**, 092905 (2008).
[15]A. Haussmann, P. Milde, C. Erler, and L. M. Eng, Nano Lett. **9**, 763 (2009).
[16]Y. Sun and R. J. Nemanich, J. Appl. Phys. **109**, 104302 (2011).
[17]Y. Sun, B. S. Eller, and R. J. Nemanich, J. Appl. Phys. **110**, 084303 (2011).
[18]Y. S. Park, J. H. Kim, and W. Yang, Surf. Interface Anal. **44**, 759 (2012).
[19]J. L. Jackel, C. E. Rice, and J. J. Veselka, Appl. Phys. Lett. **41**, 607 (1982).
[20]C. E. Rice, J. Solid State Chem. **64**, 188 (1986).
[21]Y. N. Korkishko and V. A. Fedorov, IEEE J. Sel. Top. Quantum Electron. **2**, 187 (1996).
[22]D. F. Clark, C. G. Nutt, K. K. Wong, P. J. R. Laybourn, and R. M. De La Rue, J. Appl. Phys. **54**, 6218 (1983).
[23]M. Manzo, F. Laurell, V. Pasiskevicius, and K. Gallo, Appl. Phys. Lett. **98**, 122910 (2011).

[24]M. Manzo, F. Laurell, V. Pasiskevicius, and K. Gallo, Opt. Mater. Express **1**, 365 (2011).
[25]L. Balobaid, N. C. Carville, M. Manzo, K. Gallo, and B. J. Rodriguez, Appl. Phys. Lett. **102**, 042908 (2013).
[26]N. C. Carville, M. Manzo, D. Denning, K. Gallo, and B. J. Rodriguez, J. Appl. Phys. **113**, 187212 (2013).
[27]G. Zhong, J. Jian, and Z. Wu, in *Proceedings of the 11th International Quantum Electronics Conference, IEEE Catalog No. 80 CH* (IEEE, 1980), pp. 631.
[28]J. L. Jackel, Electron. Lett. **21**, 509 (1985).
[29]A. Loni, R. W. Keys, and R. M. De La Rue, J. Appl. Phys. **67**, 3964 (1990).
[30]I. Földvári, K. Polgár, and A. Mecseki, Acta Phys. Hung. **55**, 321 (1984).
[31]R. Bhatt, S. Kar, V. Shula, P. Sen, P. K. Sen, K. S. Bartwal, and V. K. Wadhawan, Ferroelectrics **323**, 165 (2005).
[32]D. A. Bryan, R. Gerson, and H. E. Tomaschke, Appl. Phys. Lett. **44**, 847 (1984).
[33]R. Gerson, J. F. Kirchhoff, L. E. Halliburton, and D. A. Bryan, J. Appl. Phys. **60**, 3553 (1986).
[34]K. Buse, Appl. Phys. B **64**, 273 (1997).
[35]K. Buse, Appl. Phys. B **64**, 391 (1997).
[36]X. Y. Liu, H. Hatano, S. Takekawa, F. Ohuchi, and K. Kitamura, Appl. Phys. Lett. **99**, 053102 (2011).
[37]V. A. Ganshin, Yu. N. Korkishko, and V. Z. Petrova, Sov. Phys. Tech. Phys. **30**, 1313 (1985).
[38]The uncertainty in the PE depth arises from measurement error in determining the parameters of the setup, such as the angle and refractive index of the measuring prism, which directly generates uncertainties in determining the effective refractive indices of the propagating modes. The setup we used generally provides the standard deviation associated to each measured PE depth, except for the case of the two shallowest depths, where only one mode was visible and the refractive index of the layer had to be assumed to determine the thickness. For these two cases, the instrumental error was used (0.5% of the PE depth $\pm$ 5 nm).